



Cite this: *Soft Matter*, 2024, 20, 8812

Received 29th August 2024,  
Accepted 19th October 2024

DOI: 10.1039/d4sm01035c

[rsc.li/soft-matter-journal](http://rsc.li/soft-matter-journal)

## Telephone cord blister formation in solvent swollen elastomer films†

James S. Sharp, \* Nathaniel M. Roberts and Sam Walker

Video imaging was used to study large-slope folded telephone cord blister formation in solvent swollen films of polydimethylsiloxane (PDMS) elastomers. Chlorobenzene, chloroform, heptane and toluene were used to swell PDMS films with thickness values in the range  $15 \mu\text{m} < h < 223 \mu\text{m}$  supported on glass substrates. Measurements of the blister width, corrugation wavelength and blister growth speed were studied as a function of the film thickness for all four solvents. Modified theories of buckling were shown to accurately predict the film thickness dependence of the width and corrugation wavelength and a modified fracture mechanics approach was shown to reproduce the non-monotonic thickness dependence of the blister growth rates. Two critical thickness values were identified for telephone cord blisters formed on solvent swollen PDMS films—one corresponding to a lower critical thickness for blistering and the other corresponding to a peak in the thickness dependent blister growth rates. Blister formation is shown to be consistent with the existence of mixed modality in the growth of the crack tip at the film–substrate interface. Both critical thickness values are shown to depend upon the strength of the adhesive interactions between the film and the substrate and the Young's modulus of the films. A simple method of patterning surfaces with telephone cord blisters is also introduced.

## 1 Introduction

Blisters are often generated during the adhesive failure of thin films. The build-up of stress in a film can arise as a result of deposition processes<sup>1</sup> or simply due to a mismatch in physical and/or chemical properties (*e.g.* thermal contraction,<sup>1</sup> differential response to swelling solvent<sup>2–5</sup>). When the resulting areal strain energy density associated with in-plane stresses exceeds the work of adhesion between the film and substrate, delamination will occur. If there is sufficient energy remaining to bend the films then they will also buckle away from the substrate. This typically results in the formation of either circular<sup>6</sup> or straight-sided linear blisters.<sup>7–9</sup>

The formation of linear blisters only releases stress in the films in the direction perpendicular to their long axis. When large biaxial stresses are present in the film, this mode of blister formation leaves un-relaxed stress in the direction parallel to the linear blister. If large enough, these un-relaxed stresses can drive a further buckling instability in the already delaminated parts of the film to create the sinusoidal structures that are characteristic of telephone cord blisters.<sup>7–9</sup> This is

particularly true in the case where the films delaminate to create large slope folded structures where the two sides of the linear blister adhere to one another after detaching from the substrate.<sup>10,11</sup> However, telephone cord blisters do not only form in the case of these large-slope folded structures. A much more common form of telephone cord blister involves the buckling of films to form low amplitude “rucks”<sup>11</sup> that subsequently undergo secondary buckling.

Telephone cord blisters have been studied by a number of authors<sup>1,2,5,7–9,12–16</sup> and the mechanisms associated with their formation are relatively well-understood.<sup>12,13</sup> Solvent induced telephone cord blister formation in particular has received a considerable amount of recent interest.<sup>2,4,5,10</sup> The extent of solvent induced swelling in materials such as polymers can be significant, with increases in linear dimensions that range up to 40–50% of the unswollen sample dimensions.<sup>17</sup> Solvent swelling is therefore capable of generating the large biaxial stresses responsible for telephone cord blister formation in thin films that are confined on a substrate. Velankar and coworkers, in particular, have considered the effects of solvent induced swelling in polydimethylsiloxane (PDMS) films and the resulting formation of telephone cord blisters. These authors used a range of different solvents and substrate combinations.<sup>2,4</sup>

In our recent work,<sup>10</sup> we considered the effects of changing the film thickness on the buckling length scales and growth rates of telephone cord blisters in chloroform swollen films of

*School of Physics and Astronomy, University of Nottingham, Nottingham, NG7 2RD, UK. E-mail: james.sharp@nottingham.ac.uk; Tel: +44 (0)115 951 5142*

† Electronic supplementary information (ESI) available: Three movies showing the nucleation and growth of telephone cord blisters in PDMS films swollen by heptane, chlorobenzene and toluene. See DOI: <https://doi.org/10.1039/d4sm01035c>



PDMS. Prior to this only a few studies had measured and attempted to interpret the effects of changing the sample thickness on parameters such as the width, wavelength and rate of elongation (growth rate) associated with the blisters. These previous studies include measurements of the thickness dependence of the width of telephone cord and straight sided blisters in thermally deposited silicon nitride<sup>9</sup> and titanium films respectively.<sup>3</sup> Yuan and coworkers<sup>5</sup> also characterised ratios of the width and wavelength to the amplitude of blister formation.

Here we extend significantly on our previous work and describe an experimental study of the thickness dependence of telephone cord blister formation in solvent swollen thin films of PDMS supported on glass microscope slides. Swelling of the PDMS is performed in four separate solvents, namely chloroform, chlorobenzene, heptane and toluene. We also provide a more detailed analysis of the buckling and fracture mechanics phenomena that are responsible for the formation of large-slope folded telephone cord blisters.

Each of the solvents used results in a large extent of swelling being generated in the samples.<sup>17</sup> When significant swelling is coupled with confinement of the films by a substrate it results in the generation of large in-plane stresses that drive blister formation. The use of a wax release layer lowers the work of adhesion between the PDMS and the glass and results in the formation of multiple telephone cord blisters on each sample whose characteristic dimensions are shown to be largely independent of the solvent used. Simple analyses based upon previously developed theories of buckling and dynamic fracture mechanics<sup>10</sup> are shown to agree quantitatively with the data presented. Extension of the work to thinner PDMS films shows that adhesion and mechanical properties play a crucial role in determining the growth rates of the blisters. Blister growth rates are shown to have non-monotonic dependence upon film thickness which is attributed to a mixed modality in the fracture process at the growing blister crack tip. We also identify two characteristic film thickness values,  $h_c$  and  $h_0$ . The value  $h_c$  corresponds to the thickness below which telephone cord blisters do not grow and  $h_0$ , is the thickness corresponding to a peak in the thickness dependent blister growth rates.

## 2 Experimental

### 2.1 Sample preparation

Cross-linked films of polydimethylsiloxane elastomer (PDMS, Sylgard 184, Dow Corning) were prepared on Carnauba wax (Sigma Aldrich, Gillingham, UK) coated glass microscope slides by spin coating. The glass slides were initially cleaned by consecutive sonication in a surfactant solution (2% Decon Neutracon), deionised water and acetone (HPLC grade, Sigma Aldrich) for 15 minutes each. The glass slides were dried using clean lens tissues and placed on the vacuum chuck of a home-built spin coater.

Carnauba wax was dissolved at a concentration of 1 wt% in chloroform (HPLC grade, Sigma Aldrich). This was achieved by

heating the solution to 50 °C. Once all the wax had dissolved, the solution was allowed to cool to room temperature and was immediately spin coated on to the clean glass slides at a speed of 3000 rpm. This resulted in the formation of a uniform wax layer on the glass slides that was  $8 \pm 1 \mu\text{m}$  thick (as determined by weighing). Sylgard 184 was then mixed in a 10:1 ratio of resin : crosslinker, allowed to de-gas at room temperature (typically 30 minutes) and then spin coated at a range of spin speeds between 1000 rpm and 8000 rpm. A set of films with a lower Young's modulus were also prepared using a 20:1 ratio of resin : crosslinker using the same procedure. This created PDMS films with thickness values in the range  $15 \mu\text{m} < h < 223 \mu\text{m}$ . All samples were annealed in air at 110 °C for 2 hours to perform cross-linking of the PDMS. The samples were then allowed to cool to room temperature.

### 2.2 Sample imaging and data analysis

The PDMS coated glass samples were placed inside a Petri dish and illuminated from below using a 400 mW collimated white light LED (Thor Labs, MCWHL5-C1, see Fig. 1a) passed through a diffuser. The slides were quickly coated with a layer of solvent (either chlorobenzene, chloroform, heptane or toluene) using a glass pipette and the samples imaged from above using a Basler acA800-510uc camera and a UC series lens (Edmund Optics, UK) with a focal length of 25 mm. In each case an excess of solvent was used to ensure saturation of the PDMS films during swelling. All solvents were obtained from Sigma Aldrich and imaging was performed at room temperature (20 °C).

Movies of the samples were collected at a range of different frame rates (up to 200 frames per second) following the deposition of the solvents. The frame rate chosen was dependent upon the solvent being used as telephone cord blister growth rates varied considerably from solvent to solvent. A few seconds after deposition of the solvent (dependent upon film thickness and the solvent being used) a series of linear structures were observed to nucleate at multiple locations on the surface of the samples and to grow (see Movies, ESI†). It was observed that (heterogeneous) nucleation occurred preferentially near defects in the PDMS films (*e.g.* dust, scratches, other blisters). However, blisters were also observed to nucleate more slowly and homogeneously in the absence of any observable defects. These homogeneously nucleated blisters are the focus of this work.

If solvent was wicked away quickly from the samples using lens tissue paper, closer inspection revealed that the films had blistered away from the substrate to form large-slope folded structures similar to those shown in Fig. 1b. These blisters were found to be straight immediately after their formation, but were observed to buckle to form sinusoidal telephone cord-like structures as they grew (see Fig. 1c), in a manner that is consistent with previous reports of solvent swollen PDMS films.<sup>2</sup> When the imaging geometry was inverted and samples viewed from below (illuminated from above) the path taken by the blisters was observed to follow a sinusoidal path on the substrate. This indicates that the whole structure buckles and not just the delaminated parts of the film.



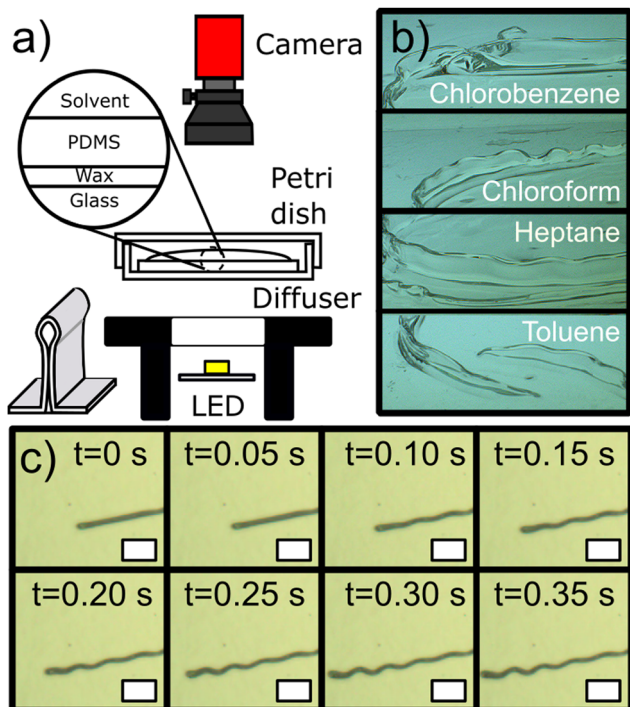


**Fig. 1** Experimental/imaging setup. Panel (a) shows a schematic diagram of the experiment. A PDMS coated glass slide is immersed in solvent and imaged from above using a camera at range of different frame rates. The bottom left of panel (a) shows a diagram of the large-slope folded structures that form during blistering of the films. Panel (b) shows examples of optical images of these large-slope folded structures that are formed during the swelling and delamination of 10 : 1 (resin : crosslinker) PDMS in all four of the solvents studied. Images were collected from an oblique angle above the level of the glass substrate and were obtained by gently wicking solvent away from the structures using a lens tissue. Panel (c) shows optical images of a growing telephone cord blister in a  $76 \pm 1 \mu\text{m}$  thick 10 : 1 PDMS film at different times as viewed from above and while still submerged in toluene. The scale bar shown in each of these images represents 1 mm.

Fig. 1(c) shows an example of a growing telephone cord blister submerged in toluene. The structures in Fig. 1(b) and (c) are of the same type. Those shown in Fig. 1b are observed from an oblique angle, following forced removal of solvent. The structures in Fig. 1(c) are observed from directly above and are still immersed in solvent. What is seen in the images in Fig. 1(c) is the top of the ridge formed by the films during folding (see the diagram in the bottom left of Fig. 1(a)).

Isolated blisters were observed to grow at a constant speed and this growth speed was found to be thickness and solvent dependent. Growth at constant speed continued until neighbouring blisters approached. This occurred as a result of two blister crack tips colliding or a crack tip approaching a pre-existing telephone cord blister. After formation, the telephone cord blisters grew until the entire surface of the sample was covered. Once a network of connected telephone cord blisters had formed, lateral growth (widening) of individual blisters occurred, resulting in the complete delamination of the PDMS films from the glass substrate. This all happened while the

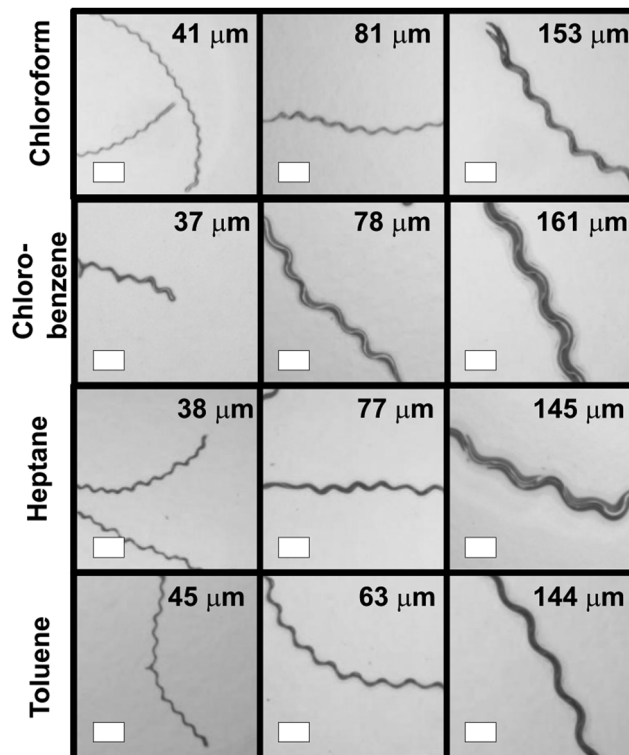


**Fig. 2** Images showing large-slope folded telephone cord blisters formed on 10 : 1 (resin : crosslinker) PDMS films during swelling with chlorobenzene, chloroform, heptane and toluene. All of the blisters are imaged from above. The scale bar represents 1 mm in each image. Thickness values of the PDMS films are given as insets in each panel.

films were immersed and before significant evaporation of solvent had taken place. Fig. 2 shows examples of telephone cord blisters that were formed by the different swelling solvents for different thickness values of PDMS. What is clear from these images is that the appearance and length scales associated with the width and buckling wavelengths of the blisters are very similar for each of the solvents used. For the most part, the blisters were observed to grow in straight lines. However Fig. 2 shows that they occasionally form arched paths. The formation of these arches correlates with the existence of defects, or the presence of a nearby solvent contact line on the PDMS films. Both of these factors influence the local stress field near the crack tip and were observed to cause the path of the blisters to deflect away from a perfectly straight trajectory.

Custom software was written in Python to analyse the movies of blister growth. Each frame in the movies was extracted, thresholded and analysed to determine the width of the blisters,  $w$ , the wavelength of the sinusoidal buckles,  $\lambda$  and the blister growth speed,  $v$ . This was done using multiple blisters on each sample. The average thickness of the samples was determined by weighing a circle of known diameter that had been cut from each PDMS film in the same region where the telephone cord blisters had been imaged. These circular sections of film were cut by placing the sample on the turntable of a spincoater and gently scoring the film as it rotated. The



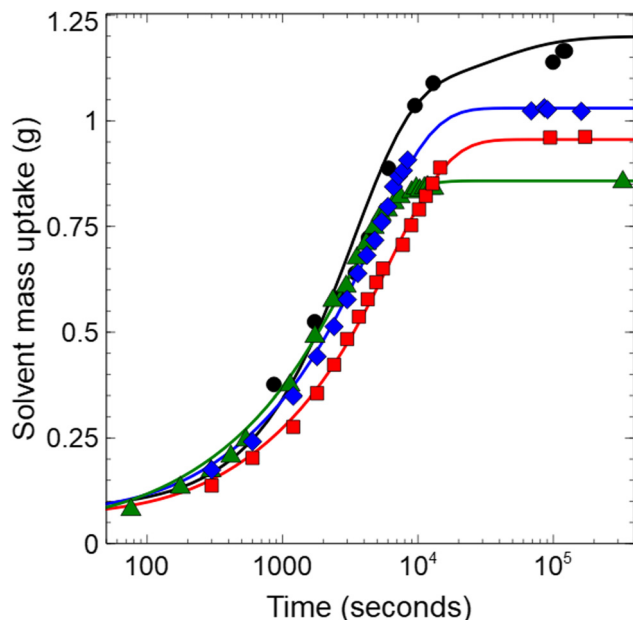


Fig. 3 Solvent mass uptake of 20 mm diameter, 3 mm thick, 10:1 (resin:crosslinker) PDMS disks as a function of time for chlorobenzene (red squares), chloroform (black circles), heptane (green triangles) and toluene (blue diamonds). Solid lines are fits to the first three terms of the expansion in eqn (1). Values obtained for the diffusion coefficient,  $D$ , are summarised in Table 1.

resulting circles were removed from the glass substrate and weighed on an analytical balance (Fisherbrand, PS-200). The thickness was then calculated assuming a density of  $1030 \text{ kg m}^{-3}$  for PDMS.

### 2.3 Solvent swelling dynamics of PDMS

Measurements of the swelling response of the PDMS were also performed by immersing 8 mm thick, 20 mm diameter disks of PDMS in the same solvents used in the telephone cord blister experiments (see Fig. 3). The disks were prepared by casting PDMS into circular polytetrafluoroethylene (PTFE) moulds and curing under identical conditions to those used to anneal the

PDMS films above. After cooling to room temperature, the disks were weighed using an analytical balance (Fisherbrand PS-200) and their dimensions measured before being immersed in the solvents. Following immersion in the solvent they were removed at regular intervals, their surfaces dried quickly with a stream of nitrogen gas, reweighed and then returned to the solvent. This process was repeated until the mass of the disks had saturated at a level within the precision of the balance used ( $\pm 0.00001 \text{ g}$ ). At this point, the dimensions of the samples were remeasured and the density of the swollen disks,  $\rho$ , and the swelling ratio,  $S$ , were calculated for each of the solvents.<sup>17</sup> Here  $S$  was calculated as the ratio of the swollen and unswollen diameters of the disks. All mass uptake data is shown in Fig. 3 and the measured values of  $\rho$  and  $S$  obtained for each solvent are given in Table 1.

### 2.4 Contact mechanics of unswollen and solvent swollen PDMS

PDMS hemispheres having a radius of  $12.2 \pm 0.1 \text{ mm}$  were prepared by casting Sylgard 184 into moulds and annealing at  $110 \text{ }^\circ\text{C}$  for 2 hours. The cured hemispheres were then immersed in the same four solvents used in the telephone cord blister studies above for 48 hours. Once the PDMS hemispheres were fully swollen, they were placed on the pan of an Ohaus P-64 analytical balance. A cleaned glass slide that had previously been coated with Carnuba wax by spin coating from chloroform (1 wt%, 3000 rpm), annealed and allowed to cool to room temperature was then pressed into contact with the solvent swollen hemispheres (see inset in Fig. 4). Images of the circular contact patch that developed during contact between the hemisphere and the glass slide were collected with the same camera used to image the telephone cord blisters. The analytical balance was used to determine the force being applied to the hemispheres. All measurements were performed with the contact patch receding (under decreasing load) to mimic the crack opening process during blister formation. The contact mechanics experiments were also performed in such a way that the rate change of the radius of the contact patch was  $\sim 0.1$  to

Table 1 Values of key parameters in the swelling of PDMS by four different solvents. Solvent diffusion coefficients ( $D$ ) were determined from mass uptake experiments and fits of eqn (1) to the data in Fig. 3. Swelling ratios ( $S$ ) of PDMS for each solvent were determined from measurements of the same sample before and after mass uptake. These values were found to be in good agreement with Lee *et al.*<sup>17</sup> Density ( $\rho$ ) was obtained from measurements of the mass and dimensions of solvent swollen PDMS disks. Values of the Young's Modulus ( $E$ ) and work of adhesion ( $\Gamma$ ) were extracted from fits of eqn (3) to the JKR contact mechanics data shown in Fig. 4. These values were obtained using either glass (g) or wax coated glass (wcg) as the substrate for PDMS and with resin to crosslinker ratios of 10:1 and/or 20:1. The parameter  $b$  was calculated using the values in this table (see main text). The value of  $\gamma$  used in the calculation of  $b$  was assumed to be the surface energy of PDMS ( $\gamma = 20 \text{ mJ m}^{-2}$ )<sup>18</sup>

	$D$ ( $\times 10^{-12} \text{ m}^2 \text{ s}^{-1}$ )	$\rho$ ( $\text{kg m}^{-3}$ )	$S$	$E$ (MPa)	$\Gamma$ ( $\text{mJ m}^{-2}$ )	$b$ ( $\text{m}^{-\frac{1}{2}}$ )
Chlorobenzene swollen 10:1 PDMS (wcg)	$223 \pm 17$	$1105 \pm 6$	$1.23 \pm 0.01$	$1.14 \pm 0.02$	$172 \pm 15$	$566 \pm 22$
Chloroform swollen 10:1 PDMS (wcg)	$231 \pm 8$	$1413 \pm 9$	$1.33 \pm 0.01$	$3.23 \pm 0.03$	$94 \pm 6$	$953 \pm 36$
Heptane swollen 10:1 PDMS (wcg)	$329 \pm 32$	$829 \pm 5$	$1.34 \pm 0.01$	$2.69 \pm 0.07$	$107 \pm 17$	$871 \pm 73$
Toluene swollen 10:1 PDMS (wcg)	$192 \pm 15$	$954 \pm 5$	$1.31 \pm 0.01$	$1.87 \pm 0.03$	$167 \pm 15$	$712 \pm 29$
Unswollen 10:1 PDMS (g)	—	$1030 \pm 5$	1	$1.84 \pm 0.08$	$232 \pm 15$	$719 \pm 50$
Unswollen 10:1 PDMS (wcg)	—	$1030 \pm 5$	1	$1.84 \pm 0.08$	$167 \pm 14$	$719 \pm 50$
Heptane swollen 20:1 PDMS (g)	—	—	$1.47 \pm 0.01$	$1.28 \pm 0.06$	$129 \pm 62$	$600 \pm 70$
Unswollen 20:1 PDMS (g)	—	$962 \pm 5$	1	$1.10 \pm 0.06$	$116 \pm 30$	$556 \pm 68$



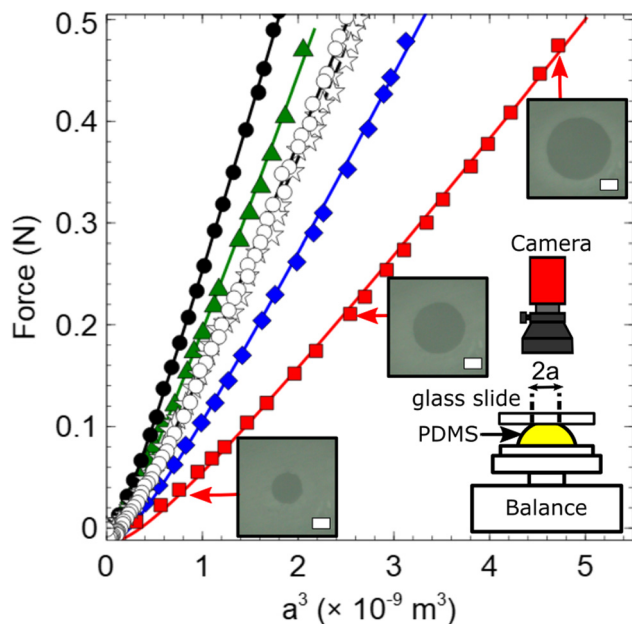


Fig. 4 Contact mechanics data for 10 : 1 (resin : crosslinker) PDMS hemispheres. The schematic diagram given as an inset shows the experimental geometry. Contact force,  $F$ , was plotted against the cube of the radius,  $a$ , of the contact patch that developed between the wax coated slides and the hemispheres (see example images shown as insets). Data are shown for unswollen PDMS in contact with glass (white circles,  $R = 12.2 \pm 0.1$  mm), unswollen PDMS in contact with wax coated glass (white stars,  $R = 12.2 \pm 0.1$  mm) as well as chlorobenzene (red squares,  $R = 15.0 \pm 0.1$  mm), chloroform (black circles,  $R = 16.2 \pm 0.1$  mm), heptane (green triangles,  $R = 16.3 \pm 0.1$  mm) and toluene (blue diamonds,  $R = 16.0 \pm 0.1$  mm) swollen hemispheres in contact with wax coated glass. Solid lines represent fits to eqn (3). Values of  $E$  and  $\Gamma$  obtained from the fits are summarised in Table 1.

$1 \text{ mm s}^{-1}$  to be comparable with the measured crack growth rates (see below).

Software written in Python was used to extract the radius of the contact patch as a function of the applied load (see main panel in Fig. 4). Similar contact mechanics measurements were also performed on unswollen PDMS hemispheres contacting cleaned glass and wax coated glass slides.

### 3 Results and discussion

Telephone cord blister formation in solvent swollen PDMS has previously been shown to be the result of excess stress build up in substrate confined films and to be limited by diffusion of solvent through the films.<sup>10</sup> Fig. 3 shows a plot of the time dependence of the mass uptake of PDMS for the four solvents used. The solid lines are fits of the mass uptake data to the equation for diffusion into a uniform slab of material<sup>19</sup>

$$m(t) = m(\infty) \left( 1 - \frac{8}{\pi^2} \sum_{n=0}^{\infty} \frac{1}{(2n+1)^2} \exp\left(-\frac{D(2n+1)^2\pi^2 t}{h_{\text{slab}}^2}\right) \right) \quad (1)$$

where  $m(\infty)$  is the mass at saturation and  $h_{\text{slab}}$  is the thickness of the sample. The values of the diffusion coefficient,  $D$ ,

obtained from the fits in Fig. 3 using the first three terms in the summation in eqn (1) are shown in Table 1. These values are in agreement with values obtained for the diffusion of similar solvents in PDMS.<sup>20</sup> What is clear from the data shown in Fig. 3 and the tabulated values of  $D$  is that the dynamics of solvent uptake in PDMS are very similar for all of the solvents studied. This is consistent with the observation that blister nucleation times were very similar for all four solvents at each PDMS film thickness.

Once the solvent has diffused through the PDMS films it reaches the wax release layer near the substrate. This wax layer has previously been postulated to reduce the work of adhesion and promote the formation of telephone cord blisters in the case of chloroform swelling.<sup>10</sup> In fact, no telephone cord blisters are observed to form when PDMS is deposited directly on to glass and swollen with the same solvents used here. Simple tests show that carnauba wax has a varying solubility in the different solvents used to swell the films in the current experiments. Toluene and chlorobenzene were found to be marginally better solvents for the wax than chloroform and heptane which showed very little evidence of dissolving small quantities of wax placed in vials of the solvents at room temperature. For reasons that are discussed below, the choice of solvents used here has very little impact on the physical dimensions (width and corrugation wavelength) of the telephone cord blisters (see Fig. 2). However, the choice of solvent has a significant effect upon the growth rates of the blisters. This behaviour is shown to be dependent upon the work of adhesion between the film and the substrate, as well as the mechanical properties of the solvent swollen films.

#### 3.1 Blister width

Fig. 5(a) shows a plot of the blister width,  $w$ , as a function of the PDMS film thickness for all four solvents used. The insets in Fig. 5(a) and (b) also show how the width is defined and measured. In each case, a position at the midpoint between two turning points on the telephone cord structure was chosen to measure the width and this was repeated at multiple locations on each blister. As shown previously, this approach to measuring the width gives values that are consistent with those measured on straight sided blisters.<sup>9</sup>

A simple analysis can be used to interpret the thickness dependence of the blister width shown in Fig. 3. This approach considers the balance of energies involved in the formation of the large-slope folded structures (see Fig. 1(b)). As shown in our previous paper,<sup>10</sup> this results in an expression for the width of the blisters,  $w$ , which scales as;

$$w \sim \sqrt{\frac{E}{24\pi^2(1-\nu^2)\gamma}} h^{\frac{3}{2}} \quad (2)$$

where  $E$  and  $\nu$  are the Young's modulus and Poisson ratio of the elastomer and  $h$  is the thickness of the PDMS film respectively. The parameter,  $\gamma$ , is the interfacial energy of PDMS. The blister  $w$  in eqn (2) therefore has the form of an elasto-capillary length.<sup>10,11,21,22</sup>



Fig. 5(a) shows the measured width data as a function of the unswollen film thickness for chloroform, chlorobenzene, heptane and toluene. It is clear from the images and data in Fig. 2 and 5 that there is little to no dependence of the blister width on the choice of solvent. The fit of the measured width data shown in Fig. 5(a) to a  $h^{\frac{3}{2}}$  power law (as predicted by eqn (2)) is shown for the combined data for 10 : 1 PDMS from all four of the solvents used and for 20 : 1 PDMS films (which have a lower value of  $E$ ) swollen in heptane. The fit yields a value for the prefactor  $b = \sqrt{\frac{E}{24\pi^2(1-\nu^2)\gamma}}$  of  $193 \pm 2 \text{ m}^{-\frac{1}{2}}$  for the 10 : 1 PDMS films and  $b = 147 \pm 8 \text{ m}^{-\frac{1}{2}}$  for the 20 : 1 PDMS films. Here we have assumed a value of  $\nu = 0.5$  for all the PDMS samples used.

### 3.2 Determination of $E$ and $\Gamma$ using contact mechanics

Contact mechanics measurements of the Young's modulus,  $E$  and work of adhesion,  $\Gamma$  were used to obtain a comparison between the fit and experimentally determined values of the prefactor in eqn (2). The Young's Modulus,  $E$ , for PDMS hemispheres was extracted from measurements of solvent swollen hemispheres in contact with wax coated surfaces. Plots of the applied force,  $F$ , vs. the cube of the radius,  $a$ , of the contact patch that developed between the hemispheres and wax coated glass were fitted using the Johnson–Kendall–Roberts (JKR) theory.<sup>23</sup> The data obtained are shown in Fig. 4 along with fits to the form of the JKR equation;

$$F = \frac{4Ea^3}{3(1-\nu^2)R} - \left(\frac{8\pi E\Gamma a^3}{1-\nu^2}\right)^{\frac{1}{2}} \quad (3)$$

where  $R$  is the radius of curvature of the hemisphere. In each case the radius of curvature of the hemispheres was calculated by multiplying the radius of curvature of the unswollen hemisphere ( $R_0 = 12.2 \text{ mm}$ ) by the swelling ratio,  $S$ , of the solvent being used. Both  $E$  and  $\Gamma$  were used as fit parameters. Table 1 gives a summary of the Young's modulus and work of adhesion values obtained for each of the hemispheres studied along with calculated values of the prefactor obtained from eqn (2). This table also shows data obtained from 20 : 1 PDMS hemispheres before and after swelling in heptane.

The values obtained for the Young's modulus,  $E$ , are consistent with those obtained by other authors for PDMS.<sup>24</sup> Values shown in Table 1 clearly show that the modulus of the swollen PDMS hemispheres depends upon the choice of swelling solvent. Previous work has attributed this variation in  $E$  to solvent leaching of small molecular weight components from the elastomers.<sup>25</sup>

The work of adhesion values that were obtained from the fits are of a similar order of magnitude to those obtained from similar elastomers in contact with glass surfaces.<sup>26,27</sup> Formally speaking, the value of  $\Gamma$  extracted from the contact measurements is the energy release rate,  $G$  (in  $\text{J m}^{-2}$ ), and is expected to be dependent upon the crack velocity.<sup>23,27</sup> For this reason, we chose to perform the contact mechanics measurements on

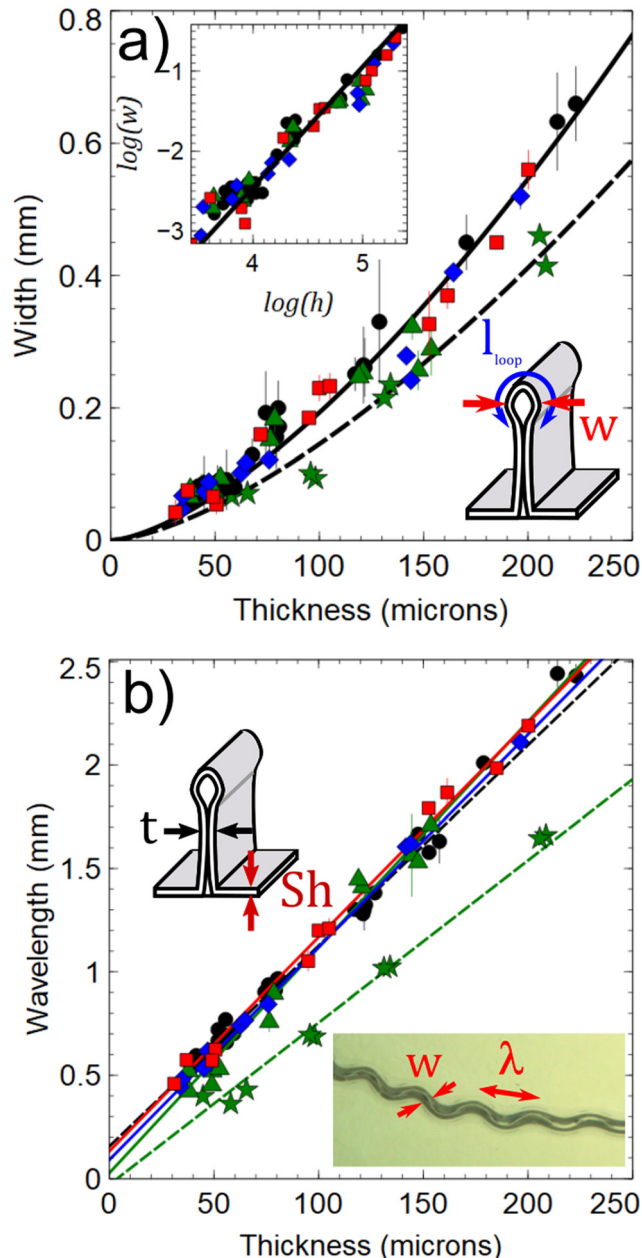


Fig. 5 Thickness dependence of blister width,  $w$ , (panel a) and buckling wavelength,  $\lambda$ , (panel b) in solvent swollen PDMS films. Data are shown as a function of the unswollen thickness of the 10 : 1 (resin : crosslinker) PDMS films for chloroform (black circles), heptane (green triangles), chlorobenzene (red squares) and toluene (blue diamonds). In addition, data are shown for 20 : 1 PDMS swollen in heptane (green stars). The solid and dashed lines in panel (a) are fits of eqn (2) to the combined data for the 10 : 1 PDMS films in all four solvents and heptane swollen 20 : 1 PDMS films respectively. A logarithmic plot shown as an inset in this panel also demonstrates the  $h^{\frac{3}{2}}$  power law dependence of the blister width. The diagram shown as an inset in panel (a) indicates how the blister width and loop length,  $l_{\text{loop}}$  are defined in reference to the large-slope folded structures that form during primary buckling. The lines in panel (b) are linear fits to the data as per eqn (4). Data and fits for chloroform are reproduced from Sharp *et al.*<sup>10</sup> The diagram shown as an inset in panel (b) defines the thickness of the large-slope folded structure used in eqn (4). An optical image (bottom right) shows how measurements of the width and wavelength are defined.



unloading in such a way that the rate of unloading and hence the crack tip velocity was of a similar order of magnitude to that observed in the blister growth experiments. Crucially, all the contact mechanics measurements were performed at the same rate of unloading which was also optimised to give the best quality data.

Consideration of the values of  $\Gamma$  obtained for unswollen PDMS hemispheres in Table 1 shows that the presence of a wax layer lowers the work of adhesion between PDMS and the substrate. This is consistent with the observation that the large-slope folded telephone cord blisters form more readily in the presence of the wax coating than on uncoated glass (where they don't form at all). Swelling of the PDMS also has the effect of reducing the work of adhesion, but to differing degrees. Solvents such as chloroform and heptane which are poor solvents for the wax layer cause significant reductions in  $\Gamma$ , while toluene and chlorobenzene (which were observed to be better solvents for the wax) have a smaller influence. Presumably, these better solvents increase the stickiness of the wax layer.

The values of  $E$  from Table 1 were combined with an estimate of the surface energy for PDMS of  $\gamma = 20 \text{ mJ m}^{-2}$  (ref. 18) and used to calculate values for the prefactor in eqn (2),

$$b = \sqrt{\frac{E}{24\pi^2(1-\nu^2)\gamma}}. \text{ These are also summarised in Table 1.}$$

Given the approximate nature of the simple scaling analysis used to derive eqn (2), the level of agreement between the tabulated values and the fit value for the prefactor

$$\left(b = 193 \pm 2 \text{ m}^{-\frac{1}{2}}\right) \text{ would seem to be acceptable. The value}$$

that was used for the surface energy of PDMS was one that had been measured in air, but the self-adhering portions of the film are immersed in solvent during large-slope fold formation. The use of values for the work of adhesion of PDMS when the films are immersed in the solvents would therefore have been more appropriate values for  $\gamma$ . However, this data was not available and it would be very difficult to measure for the films studied here. In addition, the decision to use the unswollen thickness of the PDMS films (rather than the swollen thickness  $Sh$ ) is likely to influence the calculated values. This decision was taken because parts of the large slope folded structures being imaged were protruding from the solvent. In reality some swelling of the films is still likely to occur even when they protrude in this way and this will also have an influence on the calculated values. All of these factors combined provide an explanation as to why there are differences between the calculated values of the prefactor,  $b$  and the value obtained from the fit to the width data in Fig. 5a. However, the fact that the calculated values are all within a factor of  $\sim 5$  of the value obtained from the fit to eqn (2) and that the thickness dependent data displays the same power law dependence gives us confidence that the simple scaling model captures the essential physics that determines the blister widths.

A comparison of the fits to the data for 10 : 1 and 20 : 1 PDMS in Fig. 5(a) enables a simple test of the validity of the scaling properties of eqn (2). Table 1 shows that the value of  $E$  for 20 : 1

PDMS is reduced relative to that of 10 : 1 PDMS. This is to be expected based on the lower crosslinker density in the case of the 20 : 1 composition. According to eqn (2), the fits to the width data for the 10 : 1 and 20 : 1 PDMS should vary by a factor equivalent to the square root of the ratio of the Young's moduli of the two materials. This ratio ( $1.29 \pm 0.09$ ) agrees well with the ratio of the prefactors in the fits in Fig. 5(a) ( $1.31 \pm 0.07$ ).

### 3.3 Blister wavelength

The wavelength of the sinusoidal undulations in the telephone cord blisters can be predicted by considering the competition between un-relaxed swelling stresses in the direction parallel to the large slope fold and bending stresses generated when the folded film buckles. The competition between in-plane swelling stresses and induced bending stresses results in the wrinkling of the folded films to create a characteristic undulation wavelength,  $\lambda$ , given by ref. 10;

$$\lambda = 2\pi t \sqrt{\frac{1}{12(S-1)(1-\nu^2)}} = h \sqrt{\frac{4S^2\pi^2}{3(S-1)(1-\nu^2)}} \quad (4)$$

where it is assumed that  $\nu = 0.5$  for the swollen elastomers. The thickness of the fold,  $t$  is also assumed to be  $t = 2h_s = 2Sh$  *i.e.* twice the swollen thickness of the PDMS film (see inset Fig. 5(b)) because much of the side walls of the large-slope folded structures structure remain immersed in solvent.

Fig. 5b shows a plot of the measured wavelength of the telephone cord blister corrugations as a function of the film thickness. The data shows a linear relationship for all the solvents studied in good agreement with the predictions of the simple buckling theory presented in eqn (4). Moreover, the wavelength of the telephone cord blisters is only weakly dependent upon the solvent used. This is to be expected based upon the range of values of  $S$  for 10 : 1 PDMS in the solvents used (see

Table 1) and the relatively weak dependence  $\left(\lambda \sim \sqrt{\frac{S^2}{S-1}}\right)$

predicted by eqn (4). The slopes of the plots that are predicted by eqn (4) are  $10.7 \pm 0.4$ ,  $9.7 \pm 0.3$ ,  $9.6 \pm 0.3$  and  $9.9 \pm 0.3$  for chlorobenzene, chloroform, heptane and toluene respectively using values obtained from Table 1. The fits to the data in Fig. 5(b) give corresponding values of  $10.4 \pm 0.3$ ,  $9.7 \pm 0.3$ ,  $10.9 \pm 0.4$  and  $10.3 \pm 0.3$ .

Fits to data were also obtained for 20 : 1 PDMS films swollen in heptane (dashed line in Fig. 5(b)). This composition of PDMS was shown to have a higher value of  $S$  in heptane than the 10 : 1 PDMS. As expected, the increased amount of swelling results in a reduction in the measured wavelengths. The slope of the fit to the 20 : 1 PDMS in heptane data shown in Fig. 5(b) has a value of  $9.1 \pm 0.1$ . This agrees well with the predicted value of  $9.0 \pm 0.2$  obtained using a value of  $S = 1.47$  (see Table 1) in eqn (4). The level of agreement between the fits to the data in Fig. 5b and the predicted values of the slopes according to eqn (4) is good and suggests that the theoretical approach applied to determine the buckling wavelength is appropriate.



### 3.4 Blister growth speed

Data for the crack tip speed,  $v$ , were obtained by measuring the change in the total contour length of the telephone cord blisters as a function of time (see Fig. 6). Only isolated blisters were considered and these were observed to nucleate and grow with a constant speed. In this context, an isolated blister is defined as being one that was separated by a distance of more than ten blister widths ( $10w$ ) from its nearest neighbours. When two blisters approached, their growth speeds were observed to change as a result of the overlap of the neighbouring stress fields associated with the interfacial crack tips.

The main panel in Fig. 6 contains plots of the growth speed of isolated blisters as a function of the unswollen thickness of the PDMS films for all four solvents used. This plot shows that the telephone cord blisters have an initial increase in blister growth speed, but above a critical (solvent dependent) thickness,  $h_0$ , the growth speeds start to decay. Reductions in the speed of crack growth with increasing thickness are intuitive from the perspective of an energy balance approach. Increasing thickness is expected to increase the bending energy of the films in a manner that is proportional to  $\sim h^3$ , while the in-plane strain energy generated by the swelling stresses scales as  $\sim h$  and the work of adhesion is expected to be independent of film thickness.<sup>29</sup> The stronger thickness dependence of the

bending energy in the films makes it more difficult for the film to deflect in the region of the crack tip as the films get thicker. This is expected to result in a slower rate of crack propagation. While this is observed for large film thickness values, there is clearly an additional influence on the blister growth process for thinner films. This suggests that the subtle balance of competing factors influencing crack tip opening (*e.g.* in-plane stress, out-of-plane bending/buckling and adhesion) and hence the blister growth rate are affected by the choice of solvent.

In particular, the critical thickness value at which we see a transition from increasing to decreasing growth rates in Fig. 6 correlates with changes in  $E$  and  $\Gamma$  for the solvent swollen films (see Table 1).

Arguments based upon energy release rates at the tip of the growing blister have been used to derive an expression for the speed of a crack tip growing in a film under plane-strain conditions.<sup>30</sup> In this model, the crack propagation mechanism is assumed to be largely mode I in nature (*i.e.* simple crack opening) and the speed of crack growth,  $v$ , is given by;

$$v = c_R \left( 1 - \frac{E\Gamma}{(1-\nu^2)K_0^2} \right) \quad (5)$$

where  $c_R$  is the Rayleigh wave speed,  $K_0$  is a stress intensity factor close to the crack tip and  $\Gamma$  is again the work of adhesion between the PDMS film and the substrate. If  $K_0$  is approximated by the fracture toughness,  $K_c$  (*i.e.* the critical stress intensity factor at which the crack will start to grow), then a number of authors<sup>31–33</sup> have shown that this quantity is dependent upon the thickness of a fracture specimen. Moreover, the thickness dependence has been shown to have two distinct regimes.<sup>33–35</sup>

An expression for the fracture toughness can be obtained by assuming that the growth of the telephone cord blisters is similar to that of a straight sided blister. Hutchinson and Suo<sup>28</sup> modelled the growth by considering a straight sided blister that is terminated at its growing tip by half of a circular blister (see inset Fig. 6). These authors obtained the condition for deflection of the film away from the substrate by considering the buckling of an Euler column (see inset in Fig. 6). In this model, the maximum deflection,  $\xi$ , of the film away from the substrate was shown to have the form ref. 28;

$$\xi = \sqrt{1.833 \left( \frac{\sigma}{\sigma_c^*} - 1 \right)} \quad (6)$$

where  $\sigma$  is the stress in the film and  $\sigma_c^*$  is the critical buckling stress given by

$$\sigma_c^* = 1.2235 \frac{E}{1-\nu^2} \left( \frac{h}{R} \right)^2 \quad (7)$$

Here,  $R$ , is half the width of the delaminated region of the straight sided blister and also the radius of curvature at the growing tip (see insets in Fig. 6). It is worth noting that the expressions given in eqn (6) and (7) are valid in the limit when  $h \ll R$  (*i.e.* the Euler buckling condition).

Hutchinson and Suo<sup>28</sup> showed that fracture toughness associated with the steady state growth of the linear blister

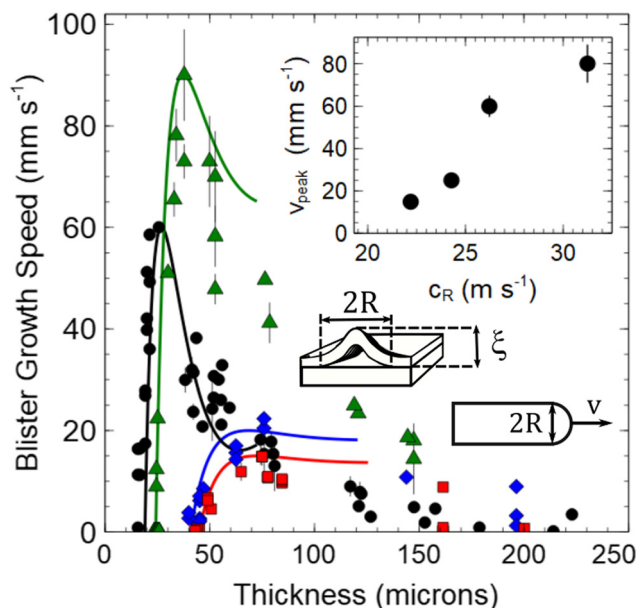


Fig. 6 Thickness dependence of the speed of the growing blister crack tip (main panel) for chloroform (black circles), heptane (green triangles), chlorobenzene (red squares) and toluene (blue diamonds) swollen 10:1 (resin: crosslinker) PDMS. The solid lines are generated using eqn (5)–(11). These are displayed over a range of thickness value where the Euler buckling condition ( $h \ll R \sim w$ ) is valid. The inset shows a plot of the peak value of the blister speed,  $v_{\text{peak}}$ , from the main panel plotted against the calculated Rayleigh speed,  $c_R = 0.95 \sqrt{\frac{E}{3\rho}}$ . Values of  $E$  and  $\Gamma$  used to generate the solid lines (main panel) and in calculation of the Rayleigh speed,  $c_R$  (inset) were obtained from Table 1. The diagrams given as insets show how the blister geometry is defined in the model of Hutchinson and Suo<sup>28</sup> (see main text).



can be written as:

$$K_0^2 = \frac{E\Gamma f(\Psi)}{\left(1 - \frac{\sigma_c}{\sigma}\right)^2} \quad (8)$$

where  $\sigma_c$  is given by

$$\sigma_c = \frac{\pi^2 E}{12(1 - \nu^2)} \left(\frac{h}{R}\right)^2 \quad (9)$$

and

$$f(\Psi) = (1 - \tan^2 \Psi) \quad (10)$$

is a function that describes the mixed mode nature of the crack formation process. The mixed mode parameter,  $\Psi$  is related to the elastic mismatch,  $\omega$ , between the film and substrate by the expression:

$$\tan(\Psi) = \frac{0.2486(1 + \nu)\xi \sin \omega + \cos \omega}{0.2486(1 + \nu)\xi \cos \omega - \sin \omega} \quad (11)$$

and  $\omega = 52.1 - 3\frac{h}{H}$  (in degrees), where  $H$  is the thickness of the substrate.<sup>28</sup>

The solid lines in the main panel of Fig. 6 were generated by combining eqn (5)–(11). These are truncated because of the range of validity of the Euler condition. Stress in the films was calculated using  $\sigma = E(S - 1)$  and the elastic mismatch was approximated to  $\omega \sim 52.1$  because  $H \gg h$  for the system studied here. A value of  $\nu = 0.5$  was assumed for the swollen PDMS films and the width of the delaminated region was set to be equal to the width of the blisters *i.e.*  $2R = w = bh^{\frac{3}{2}}$ . It is worth noting that only  $c_R$  was as a free parameter when generating the solid lines in Fig. 6. All other parameters were determined using measured values obtained Table 1. Agreement between the model and the crack speed data is generally good.

The inset in Fig. 6 shows the measured peak growth speed,  $v_{\text{peak}}$  (as defined in the inset in Fig. 7) plotted against the calculated Rayleigh speed ( $c_R = 0.95\sqrt{\frac{E}{3\rho}}$ ). According to the above model  $v_{\text{peak}}$  should be equal to  $c_R$ . However, this is clearly not the case. While the value of  $v_{\text{peak}}$  is linearly related to the Rayleigh speed, it is approximately 300 times smaller than the calculated value of  $c_R$  obtained using the values in Table 1. The reasons for this are not entirely clear as  $c_R$  should set the magnitude of the velocity of the blister crack tip velocity. Despite the discrepancies in the magnitude of the crack speeds, the functional form of the lines that are generated by eqn (5)–(11) agree well with the experimental data over the range of validity of the Euler buckling approach used. Modelling the crack speed for thicker films would require a more detailed analysis which is beyond the scope of the current work. However, we note that the general trend of decreasing crack speed with increasing thickness observed in the data is consistent with the intuitive predictions discussed above.

There are a number of limitations of the theoretical approach used above that warrant further discussion and which may account for the discrepancies identified above.

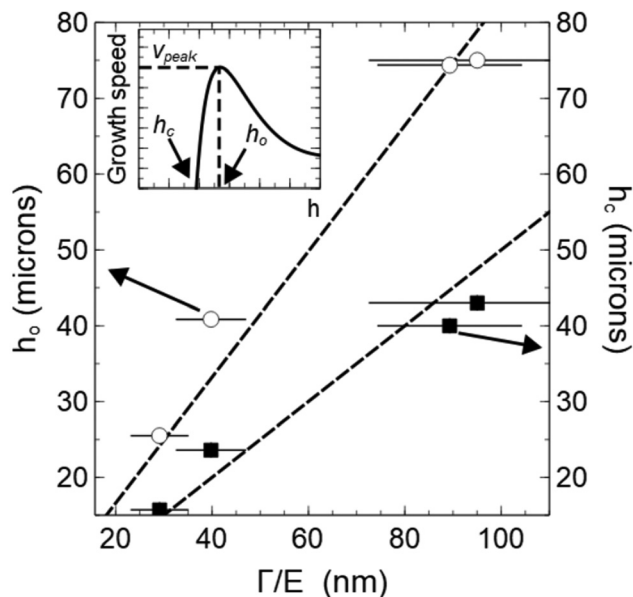


Fig. 7  $\Gamma/E$  dependence of the thickness corresponding to the peak growth speed,  $h_0$  (left axis), and the critical thickness,  $h_c$  (right axis), below which blisters do not grow for solvent swollen PDMS films. The dashed lines are linear fits to the  $h_c$  and  $h_0$  data. The diagram/plot given as an inset shows how  $h_0$ ,  $h_c$  and  $v_{\text{peak}}$  are defined.

Firstly the use of the width,  $w$ , in determining the radius of curvature of the growing crack tip is potentially problematic. If we look at the images in Fig. 1(b), there is some suggestion that the radius of curvature at the growing tip is smaller than the width of the blisters. Moreover, the expressions used for the fracture toughness (eqn (8)–(11)) assume that the extent of mode mixing is the same at all points on the growing blister tip. The expression used for the crack speed also assumes that crack opening is dominated by mode I fracture. Studies by Hutchinson and Suo<sup>28</sup> and Faou *et al.*<sup>8</sup> have both shown that the degree of mode mixing is heterogeneous near the edge of a growing telephone cord blister and that shear deformations (*i.e.* mode II fracture) play an appreciable role in the crack opening process. Finally, the use of a model involving straight sided blisters is also a potential limitation. The stress field distribution close to the tip of an undulating blister is different to that experienced by a straight sided one.<sup>8</sup>

The data obtained for the growth speed of the blisters shown in Fig. 6 shows that there is a lower critical thickness,  $h_c$  (see inset in Fig. 7), below which the blisters do not grow. This is to be expected from an energetic perspective if the strain energy stored in the film is insufficient to overcome adhesive forces between the film and substrate. When both energies are equal we expect that  $\frac{E\varepsilon^2 h_c}{2(1 - \nu^2)} = \Gamma$ , where  $\varepsilon = S - 1$  is the strain in the film. Rearranging this equation gives the result that,

$$h_c = \frac{2\Gamma(1 - \nu^2)}{E(S - 1)^2} \propto \frac{\Gamma}{E} = l_{EA} \quad (12)$$

where  $l_{EA}$  is the elasto-adhesive length. A similar result can be



obtained by taking the limit where the stress in the film is equal to the critical stress *i.e.*  $\sigma = \sigma_c^*$  and setting  $R = w = bh^{1.5}$  in eqn (7).

The main panel in Fig. 7 confirms that  $h_c$  is proportional to  $\frac{\Gamma}{E}$  for the solvent swollen PDMS samples studied here. However, the slope of the linear fit shown is roughly an order of magnitude larger than that predicted by eqn (12) when the values obtained from Table 1 are used on the horizontal axis. One possible reason for this is that the simple analysis above neglects the energy of bending the film which is also expected to determine the ability of films to detach and the blister crack tip to open. Including an additional energy term would mean that more strain energy (and hence thicker films) is required to drive crack propagation at the interface between the film and substrate.

The peak in the thickness dependent growth speed data (Fig. 6) occurs at a film thickness,  $h_0$  which is slightly larger than  $h_c$ . According to the model introduced above, the non monotonic thickness dependence is caused by the functional form of the fracture toughness in eqn (8), specifically through the function  $f(\Psi)$ . This suggests that the relative contributions of different modes of fracture change as the thickness increases. Note that  $\Psi$  from eqn (11) is defined in such a way that  $\tan \Psi = \frac{K_{II}}{K_I}$  *i.e.* the ratio of the mode II (shear) and mode I (normal) stress intensity factors. A plot of the thickness dependence of eqn (11) (not shown) shows that the contribution of shear stresses peaks at  $h = h_0$  and then decays, with mode II fracture dominating crack tip propagation over the range of film thickness values studied.

Fig. 7 shows that  $h_0$  also scales linearly with  $\frac{\Gamma}{E}$  for the swollen PDMS films. This is perhaps unsurprising given that the same subtle balance of adhesive and elastic energies influences crack opening. However, the slope of the fit to the data for  $h_0$  in Fig. 7 is a factor of  $\sim \sqrt{3}$  larger than that obtained for  $h_c$ . This is again indicative of the increased importance of shear stresses at  $h = h_0$  as the shear modulus  $G = \frac{E}{3}$  (for a material with  $\nu = 0.5$ )<sup>36</sup> and the shear equivalent of the elasto-adhesion length  $\left(\frac{\Gamma}{G}\right)$  would result in a larger thickness scale. Again we note that shear stress plays a role at all film thickness values according to eqn (11) *i.e.* crack opening is never purely mode I. As a result we expect the values of  $h_0$  to lie somewhere in the range  $h_c < h_0 \leq 3h_c$  depending upon the degree of mode mixing involved in crack/blister propagation.

Finally, we consider the role played by the wax layer in the process of telephone cord blister formation. As discussed previously, this layer has the effect of lowering the work of adhesion between the PDMS and the glass, but the question remains as to whether it influences the morphology and growth rates of the growing blisters? The carnauba wax used in these experiments forms a semi-crystalline layer on the surface after spin coating and the resulting roughness of this layer might be expected to influence blister nucleation and growth. A simple

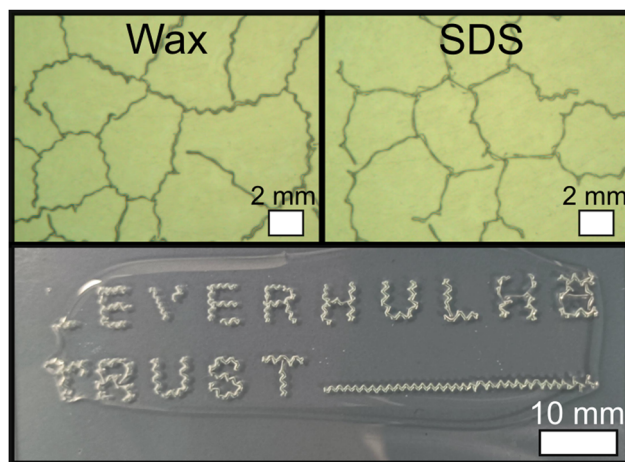


Fig. 8 The role of the intermediate wax layer. The top two panels show telephone cord blisters that were formed in  $45 \pm 5 \mu\text{m}$  thick 10 : 1 PDMS films. The image on the left shows blisters that were formed on wax coated glass and the right hand image shows blisters formed on glass spin coated with a sodium dodecylsulfate (SDS) surfactant layer. The bottom panel shows the results of a simple patterning experiment where lines of SDS solution were drawn on to a glass slide prior to deposition of the PDMS.

test was performed where we spin coated simple surfactant solution (1 wt% sodium dodecylsulfate (SDS) in methanol) as an alternative to the carnauba wax. This was shown to have the same effect of reducing the work of adhesion relative to an uncoated glass substrate as the wax layer. There were no observable differences in the morphology, density and/or the growth rates of blisters that formed on the SDS coated glass substrates (see top panels in Fig. 8). This suggests that the wax layer does not have a significant influence on blister formation other than by lowering the energy of adhesion between the film and the glass.

In hindsight, there are a number of advantages to using a spin coated surfactant solution rather than the wax layer. Sample preparation is easier and it removes any potential uncertainties relating to the effects of the (crystallinity induced) roughness. We have also shown that the use of SDS provides a potentially interesting way of patterning surfaces with telephone cord blisters. Simple experiments where we replaced the ink in a fine-tip marker with SDS dissolved in methanol, showed that we were able to pattern regions with a lower work of adhesion by simply drawing the surfactant solution on to glass prior to deposition of the PDMS. This allowed us to pattern the subsequent formation of telephone cord blisters (see bottom panel in Fig. 8). In addition to having interesting patterning applications, this approach also provides a way of controlling the formation of telephone cord blisters that will permit the interactions between them to be studied. For example, future measurements will look at how the width of the patterned tracks (different sized marker tips), the angle of approach between blisters and their separation influences their widths, wavelengths and growth speeds.

In summary, the work presented here has considered the effects of solvent induced swelling and telephone cord blister



formation in PDMS films. The buckling length scales (blister width and undulation wavelength) have been shown to be insensitive to the choice of solvents used in this study. This is largely attributed to the similarities in the swelling ratios obtained for PDMS in the solvents. However, the blister growth speeds were shown to be sensitive to the choice of solvent. The non-monotonic thickness dependence of the blister growth speeds allowed us to identify a critical lower thickness,  $h_c$ , below which blister formation does not occur and a second thickness,  $h_0$ , where shear stresses dominate the mixed mode fracture associated with the growing blister crack tip.

## 4 Conclusion

The thickness dependence of telephone cord blister formation in solvent swollen films of PDMS was studied using video imaging. Measurements of the thickness dependence of the width, wavelength and growth speeds were obtained and compared to theories of thin film buckling, delamination and dynamic fracture mechanics respectively. Data for the width and wavelength were found to be in good agreement with previously developed theories of buckling in thin films and insensitive to the choice of solvent. A modified theory of blister growth was also developed and shown to be in good agreement with the thickness dependence of the blister growth speed in PDMS films that had been swollen in different solvents. A non-monotonic thickness dependence of the blister growth rates was observed and interpreted in the context of mixed modality of fracture at the growing crack tip. Two characteristic thickness values associated with interfacial fracture were identified and found to scale with the elasto-adhesive length. Patterning of adhesive interactions was also shown to give spatial control over the formation of telephone cord blisters.

## Author contributions

J. S. S. was responsible for data collection, analysis and writing the manuscript. N. M. R. was responsible for collecting data (specifically the data for films swollen in chloroform) and S. W. helped design and built the contact mechanics experimental apparatus.

## Data availability

The data supporting this article have been included in the manuscript and as part of the ESI.†

## Conflicts of interest

There are no conflicts to declare.

## Acknowledgements

The authors gratefully acknowledge financial support from the Leverhulme Trust under research project grant RPG-2021-337.

## Notes and references

- 1 S.-J. Yu, S.-C. Li, Y. Ni and H. Zhou, *Acta Mater.*, 2017, **127**, 220–229.
- 2 S. S. Velankar and V. Lai, *ACS Appl. Mater. Interfaces*, 2012, **4**, 24–29.
- 3 X. Xue, S. Wang, C. Zeng, L. Li and C. Li, *Surf. Interface Anal.*, 2018, **50**, 180–187.
- 4 D. Breid, V. Lai, A. T. Flowers, X. Guan, Q. Liu and S. S. Velankar, *Langmuir*, 2021, **37**, 6985–6994.
- 5 B. Yuan, C. M. Harvey, K. Shen, R. Thomson, G. W. Critchlow, D. Rickerby, S. Yu and S. Wang, *Compos. Struct.*, 2022, **280**, 114909.
- 6 J. S. Sharp and R. A. L. Jones, *Adv. Mater.*, 2002, **14**, 799–802.
- 7 B. Audoly, *Phys. Rev. Lett.*, 1999, **83**, 4124–4127.
- 8 J.-Y. Fao, G. Parry, S. Grachev and E. Barthel, *Phys. Rev. Lett.*, 2012, **108**, 116102.
- 9 Y.-D. Sun, Q.-X. Chen, Y.-F. Feng, J. Chen and S.-J. Yu, *Surf. Rev. Lett.*, 2015, **22**, 1550046.
- 10 J. S. Sharp and N. M. Roberts, *Soft Matter*, 2023, **19**, 7796–7803.
- 11 B. Davidovitch and V. Demery, *Eur. Phys. J. E: Soft Matter Biol. Phys.*, 2021, **44**, 11.
- 12 Y. Ni, S. Yu, H. Jiang and L. He, *Nat. Commun.*, 2017, **8**, 14138.
- 13 B. Yuan, C. M. Harvey, R. C. Thomson, G. W. Critchlow, D. Rickerby and S. Wang, *Compos. Struct.*, 2019, **225**, 111108.
- 14 G. Gioia and M. Ortiz, *Acta Mater.*, 1998, **46**, 169–175.
- 15 Q. Wang, C. Wang, Z. Wang, J. Zhang and D. He, *Appl. Surf. Sci.*, 2008, **255**, 1836–1840.
- 16 P. Cai, S. Yu, X. Xu, M. Chen, C. Sui and G.-X. Ye, *Appl. Surf. Sci.*, 2009, **255**, 835–8358.
- 17 J. N. Lee, C. Park and G. M. Whitesides, *Anal. Chem.*, 2003, **75**, 6544–6554.
- 18 S. Wu, in *Polymer Handbook*, ed. J. Brandrup, E. H. Immergut and E. A. Grulke, Wiley-Interscience, New Jersey, 4th edn, 1994, ch. VI, vol. 2, pp. 521–542.
- 19 J. Crank, *The Mathematics of Diffusion*, Oxford University Press, Oxford, 2nd edn, 1975.
- 20 E. Favre, P. Schaetzel, Q. T. Nguyen, R. Clement and J. Neel, *J. Membr. Sci.*, 1994, **92**, 169–184.
- 21 C. Py, P. Reverdy, L. Doppler, J. Bico, B. Roman and C. N. Baroud, *Phys. Rev. Lett.*, 2007, **98**, 156103.
- 22 A. E. Cohen and L. Mahadevan, *Proc. Natl. Acad. Sci. U. S. A.*, 2003, **100**, 12141–12146.
- 23 K. R. Shull, *Mater. Sci. Eng., R*, 2002, **36**, 1–45.
- 24 I. Johnston, D. K. McCluskey, C. K. L. Tan and M. C. Tracey, *J. Micromech. Microeng.*, 2014, **24**, 035017.
- 25 J. D. Glover, C. E. McLaughlin, M. K. McFarland and J. T. Pham, *J. Polym. Sci.*, 2020, **58**, 343–351.
- 26 D. Baek, S. Saito and K. Takahashi, *J. Adhes. Sci. Technol.*, 2017, **32**, 158–172.
- 27 D. A. Bellido-Aguilar, M. Safaripour, K. VanDonselaar, L.-S. C. Nduagum, D. C. Webster and A. B. Croll, *Adv. Eng. Mater.*, 2023, **25**, 2300098.



- 28 J. W. Hutchinson and Z. Suo, *Adv. Appl. Mech.*, 1991, **29**, 63–191.
- 29 S. P. Timoshenko and J. M. Gere, *Theory of Elastic Stability*, Dover, Mineola, New York, 2nd edn, 2009.
- 30 L. B. Freund, *Dynamic Fracture Mechanics*, Cambridge University Press, Cambridge, 1st edn, 1990.
- 31 G. T. Hahn, R. G. Hoagland, A. R. Rosenfield and R. Sejnoha, *Metall. Trans.*, 1974, **5**, 475–482.
- 32 M. O. Lai and W. G. Ferguson, *Eng. Fract. Mech.*, 1986, **23**, 649–659.
- 33 J. I. Bluhm, *Proc. ASTM*, 1961, **61**, 1324–1330.
- 34 E. I. Preiß, B. Merle and M. Göken, *Mater. Sci. Eng., A*, 2017, **691**, 218–225.
- 35 H.-W. Wang, Y.-L. Kang, Z.-F. Zhang and Q.-H. Qin, *Int. J. Fract.*, 2003, **123**, 177–185.
- 36 D. Tabor, *Gases, Liquids and Solids and other states of matter*, Cambridge University Press, Cambridge, 3rd edn, 1993.

